

# Bayesian Filtering of Smooth Signals: Application to Altimetry

Abderrahim Halimi<sup>(1)</sup>, Gerald S. Buller<sup>(1)</sup>, Steve McLaughlin<sup>(1)</sup>, Paul Honeine<sup>(2)</sup>

## Abstract

This paper presents a novel Bayesian strategy for the estimation of smooth signals corrupted by Gaussian noise. The method assumes a smooth evolution of a succession of continuous signals that can have a numerical or an analytical expression with respect to some parameters. The Bayesian model proposed takes into account the Gaussian properties of the noise and the smooth evolution of the successive signals. In addition, a gamma Markov random field prior is assigned to the signal energies and to the noise variances to account for their known properties. The resulting posterior distribution is maximized using a fast coordinate descent algorithm whose parameters are updated by analytical expressions. The proposed algorithm is tested on satellite altimetric data demonstrating good denoising results on both synthetic and real signals. The proposed algorithm is also shown to improve the quality of the altimetric parameters when combined with a parameter estimation strategy.

## Index Terms

Altimetry, Bayesian algorithm, coordinate descent algorithm, gamma Markov random fields

## I. INTRODUCTION

In many applications, the development of new sensor technologies allows for high speed acquisition of a succession of signals leading to a slight variation from one signal to the next. This is the case for satellite altimetric signals that can be described as a succession of continuous functions corrupted by noise [1]–[3]. Indeed, when observing the ocean, the

<sup>(1)</sup> Heriot-Watt University, School of Engineering and Physical Sciences, Edinburgh, U.K (e-mail: {A.Halimi,G.S.Buller,s.mclaughlin}@hw.ac.uk).

<sup>(2)</sup> The LITIS lab, Université de Rouen, Rouen, France (e-mail: paul.honeine@univ-rouen.fr)

This work was supported by the EPSRC Grants EP/J015180/1, EP/N003446/1, and EP/K015338/1

altimetric successive signals show a reduced variation due to the nature of ocean (see Fig. 1 that shows a succession of 800 signals acquired by the Jason-2 mission). This paper aims to exploit this correlation to denoise the observed altimetric signals.

A satellite altimeter is a nadir-viewing radar that emits regular pulses and records the travel time, the magnitude and the shape of each return signal after reflection on the Earth's surface. This reflected echo provides information about some physical parameters such as the range between the satellite and the observed scene (denoted by  $\tau$ ), the significant wave height (denoted by SWH) and the wind speed (related to the signal's amplitude  $P_u$ ). However, altimetric signals are corrupted by speckle noise and many recent studies and missions have been focusing on improving the quality of these signals by reducing the noise effect. This goal is generally achieved by considering two main approaches. The first approach improves the altimetric technology by increasing the number of observations (as for the Altika mission [4]) or by using a new delay/Doppler processing [5]. The second approach improves the processing of the observed signals by considering more sophisticated physical models [2], [3], [6], [7], or improved signal processing algorithms [8], [9]. This paper focuses on signal processing approaches that can be divided into two categories. The first operates on the estimation algorithm to incorporate the known smooth properties of the altimetric parameters [8]–[10] while the second operates on the observed signals to reduce the effects of noise [11], [12]. This latter approach will be considered in this paper, i.e., noise reduction in the observed altimetric signals. The main motivation for this choice is to propose a denoising algorithm that is independent from the parameter estimation algorithm, thus, it can be easily combined with any existing estimation algorithms [6], [8]–[10] leading to an improvement in parameter estimation.

The first contribution of this paper is a hierarchical Bayesian model to denoise a set of smooth signals. Each signal is assumed corrupted by additive, independent and non-identically distributed Gaussian noise. This noise model generalizes the independent and identically distributed (i.i.d.) Gaussian noise that is generally assumed when considering altimetric data [6], [13]. A gamma Markov random field (GMRF) prior [14] is considered to account for the correlation between the noise variances to better approximate the speckle noise. The signal energies are also assigned a GMRF prior to better approximate their continuity. Using Bayes rule, the likelihood and the prior distributions lead to a posterior distribution that will be used to estimate the noiseless signals and the noise parameters (as described in the next paragraph). Note that the proposed Bayesian hierarchy is generic in the sense that it does not

assume a specific signal model. Indeed, the signal can be expressed by a numerical formula or given by linear/nonlinear analytical function with respect to (w.r.t.) some parameters.

The second contribution of this paper is the derivation of a denoising algorithm associated with the proposed hierarchical Bayesian model. The minimum mean square error (MMSE) and maximum a posteriori (MAP) estimators of the unknown signals/parameters cannot be easily computed from the obtained joint posterior. In this paper, the MAP estimator is evaluated by considering a coordinate descent algorithm (CDA) [10], [15], [16] whose convergence to a stationary point is ensured. The proposed algorithm sequentially updates the estimated noiseless signals, noise variances and other hyperparameters by analytical formulas leading to a reduced computational cost. The proposed Bayesian model and estimation algorithm are validated using synthetic and real altimetric data acquired during the Jason-2 mission. The obtained results are very promising and show the potential of the proposed denoising strategy.

The paper is organized as follows. Section II introduces the observation model and the considered altimetric signal. The proposed hierarchical Bayesian model and its estimation algorithm are introduced in Sections III and IV. Section V validates the proposed technique using simulated data with controlled ground truth. Section VI shows results obtained using real data resulting from the Jason-2 mission. Finally, conclusions and future work are reported in Section VII.

## II. PROBLEM FORMULATION

Consider  $M$  successive signals  $\mathbf{S} \in \mathbb{R}^{K \times M}$  and let  $\mathbf{Y} \in \mathbb{R}^{K \times M}$  denote their noisy version. Let  $\mathbf{y}_{:m} \in \mathbb{R}^{K \times 1}$  be the  $m$ th column of  $\mathbf{Y}$  and  $\mathbf{y}_{k:} \in \mathbb{R}^{1 \times M}$  its  $k$ th row, representing the  $k$ th temporal gate for all signals. For notation simplicity, we denote  $\mathbf{y}_{:m} = \mathbf{y}_m$ , for  $m = 1, \dots, M$  and  $\mathbf{y}_{k:} = \mathbf{y}_k$ , for  $k = 1, \dots, K$  (the same notation is used for  $\mathbf{s}$ ). The observation model is given by

$$\mathbf{y}_m = \mathbf{s}_m(\boldsymbol{\Theta}_m) + \mathbf{e}_m, \text{ with } \mathbf{e}_m \sim \mathcal{N}(\mathbf{0}_K, \boldsymbol{\Sigma}) \quad (1)$$

where  $\sim$  means “is distributed according to”,  $\mathbf{y}_m$  and  $\mathbf{s}_m$  are  $(K \times 1)$  vectors representing the  $m$ th observed and noiseless signals, and  $\mathbf{e}_m$  is a centered Gaussian noise vector with a diagonal covariance matrix  $\boldsymbol{\Sigma} = \text{diag}(\boldsymbol{\sigma}^2)$  with  $\boldsymbol{\sigma}^2 = (\sigma_1^2, \dots, \sigma_K^2)^T$  a  $(K \times 1)$  vector. The signals  $\mathbf{S}$  might depend on some parameters (by a linear or nonlinear expression) which are denoted by the  $(1 \times H)$  vector  $\boldsymbol{\Theta}_m = [\theta_1(m), \dots, \theta_H(m)]$  containing the  $H$  parameters of the  $m$ th signal. Note, however, that the proposed method does not necessarily require a parametric expression for  $\mathbf{S}$ , and is valid provided that the signals satisfy some properties (as described in the following). In different applications such as oceanic altimetry [8], [9], the successive signals show a reduced variation mainly because of the correlation between the successive physical parameters  $\boldsymbol{\Theta} = (\boldsymbol{\Theta}_1^T, \dots, \boldsymbol{\Theta}_M^T)^T$  (see Fig. 1). This smooth variation can be highlighted by expressing the observed signals (1) as follows

$$\mathbf{y}_k = \mathbf{s}_k(\boldsymbol{\Theta}) + \mathbf{e}_k, \text{ with } \mathbf{e}_k \sim \mathcal{N}(\mathbf{0}_M, \sigma_k^2 \mathbb{I}_M) \quad (2)$$

where  $k \in \{1, \dots, K\}$  indexes the signal samples that are known as “temporal gates”,  $\mathbb{I}_M$  denotes the  $(M \times M)$  identity matrix and  $\mathbf{s}_k$  is a smooth  $(M \times 1)$  vector representing the signal evolution at the  $k$ th gate (see Fig. 1 (bottom) for examples). The proposed Bayesian method aims to filter the observed signals  $\mathbf{y}_k$ ,  $k \in \{1, \dots, K\}$ , to retrieve the noiseless signals  $\mathbf{s}_k$ ,  $k \in \{1, \dots, K\}$ . The next section introduces the satellite altimetric model that will be considered in this paper since it satisfies the model described above.

### A. Conventional altimetric model

The altimetric model, in its simplified version, accounts for three parameters that are the amplitude  $P_u$ , the epoch  $\tau$  and the significant wave height SWH. The resulting mathematical nonlinear model for the altimetric signal is known as the “Brown model” and is given by [2], [6]

$$s(t) = \frac{P_u}{2} \left[ 1 + \text{erf} \left( \frac{t - \tau_s - \alpha \sigma_c^2}{\sqrt{2} \sigma_c} \right) \right] \exp \left[ -\alpha \left( t - \tau_s - \frac{\alpha \sigma_c^2}{2} \right) \right] \quad (3)$$

where

$$\sigma_c^2 = \left( \frac{\text{SWH}}{2c} \right)^2 + \sigma_p^2 \quad (4)$$

and where  $\text{erf}(t) = \frac{2}{\sqrt{\pi}} \int_0^t e^{-z^2} dz$  stands for the Gaussian error function,  $t$  is the time,  $\tau_s = \frac{2\tau}{c}$  (resp.  $\tau$ ) is the epoch expressed in seconds (resp. meters),  $c$  is the speed of light,  $\alpha$  and  $\sigma_p^2$  being two known parameters (depending on the satellite and on the measurement instrument). The nonlinear model described in (3) is commonly used in the altimetric community mainly because of its simplicity [3], [6], [10]. Note that the discrete altimetric signal is gathered in the vector  $\mathbf{s} = (s_1, \dots, s_K)^T$ , where  $K = 104$  gates,  $s_k = s(kT)$ ,  $T$  is the time resolution and  $\Theta_m = [\theta_1(m), \theta_2(m), \theta_3(m)] = [\text{SWH}(m), \tau(m), P_u(m)]$  is a  $(1 \times 3)$  vector containing the 3 altimetric parameters SWH,  $\tau$ ,  $P_u$  for the  $m$ th signal.

The altimetric signals are corrupted by speckle noise that, thanks to the averaging that takes place on-board of the satellite, can be approximated by additive Gaussian noise as shown in [10], [17]–[19]. Thus, the observation altimetric model satisfies (2). Moreover, the noise variances obtained,  $\sigma_k^2, k \in \{1, \dots, K\}$ , after the satellite averaging, are correlated due to the nature of the speckle noise (this correlation will be considered in the proposed Bayesian scheme). Note that this paper only considers oceanic observations which generally show a smooth variation between successive signals. The next section introduces the Bayesian model associated with a set of  $M$  successive signals considered in this paper.

### III. HIERARCHICAL BAYESIAN MODEL

This section introduces a hierarchical Bayesian model to denoise  $M$  successive signals. The Bayesian approach first requires the determination of the likelihood that is based on the statistical model associated with the observed data. Second, the known properties of the parameters of interest are modeled via suitable prior distributions. Bayes theorem allows the likelihood and the priors to be combined to build the posterior distribution of the statistical model. More precisely, if  $f(\mathbf{X})$  denotes the prior distribution assigned to the parameter  $\mathbf{X}$ , the Bayesian approach computes the posterior distribution of  $\mathbf{X}$  using Bayes rule

$$f(\mathbf{X}|\mathbf{Y}) = \frac{f(\mathbf{Y}|\mathbf{X})f(\mathbf{X})}{f(\mathbf{Y})} \propto f(\mathbf{Y}|\mathbf{X})f(\mathbf{X}) \quad (5)$$

where  $\propto$  means “proportional to” and  $f(\mathbf{Y}|\mathbf{X})$  is the likelihood of the observation vector  $\mathbf{Y}$ . The parameter  $\mathbf{X}$  is then estimated from this posterior distribution by computing its mean (MMSE estimator) or its maximum (MAP estimator). The following sections introduce the likelihood and the prior distributions considered in this paper. The unknown parameters of

the proposed model include the  $(K \times M)$  matrix representing the noiseless signals  $\mathbf{S}$ , and the  $(K \times 1)$  vector  $\boldsymbol{\sigma}$  containing the noise variances associated with the  $M$  considered signals.

#### A. Likelihood

The observation model defined in (2) and the Gaussian properties of the noise sequence  $\mathbf{e}_k$ ,  $k \in \{1, \dots, K\}$ , yield

$$f(\mathbf{y}_k | \mathbf{s}_k, \sigma_k^2) \propto \left( \frac{1}{\sigma_k^2} \right)^{\frac{M}{2}} \exp \left( -\frac{\|\mathbf{y}_k - \mathbf{s}_k\|^2}{2\sigma_k^2} \right) \quad (6)$$

where  $\|\cdot\|$  denotes the standard  $l_2$  norm such that  $\|\mathbf{x}\|^2 = \mathbf{x}^T \mathbf{x}$  and  $\mathbf{s}_k(\boldsymbol{\Theta})$  has been denoted by  $\mathbf{s}_k$  for brevity. Assuming independence between the temporal samples of the observed signals leads to

$$f(\mathbf{Y} | \mathbf{S}, \boldsymbol{\Theta}) \propto \prod_{k=1}^K f(\mathbf{y}_k | \mathbf{s}_k, \sigma_k^2). \quad (7)$$

#### B. Priors for the observed signal

As previously assumed, the successive observed signals evolve slowly leading to smooth vectors  $\mathbf{s}_k$ , for  $k \in 1, \dots, K$  (see Fig. 1 (bottom)). This property is satisfied by considering a Gaussian prior for  $\mathbf{s}_k$  ensuring smoothness as follows

$$\mathbf{s}_k | \epsilon_k^2 \sim \mathcal{N}(\mathbf{0}_M, \epsilon_k^2 \mathbf{H}), \quad (8)$$

where  $\mathbf{H}$  is an  $(M \times M)$  matrix representing the squared-exponential covariance function given by  $H(m, m') = \exp \left[ -\frac{(m-m')^2}{(30)^2} \right]$ , which introduces the correlation between the successive signals and  $\epsilon_k^2$  is a variance parameter that is gate dependent. From (8), it is clear that this variance is related to the energy of the signals at the  $k$ th gate (via the norm  $\mathbf{s}_k^T \mathbf{H}^{-1} \mathbf{s}_k$ ). Moreover, because of the continuity of the signal  $\mathbf{s}_m$  w.r.t. the temporal gates, the signal energies vary smoothly from one gate to another. Therefore, we expect  $\epsilon_k^2$  to vary smoothly from one gate to another which will be introduced by considering a specific prior for  $\epsilon_k^2$ , as explained in Section III-D.

#### C. Prior for the noise variance

Due to the speckle origins of the corrupting noise, we expect the noise variances  $\sigma_k^2$ ,  $k \in \{1, \dots, K\}$  to vary smoothly. This behavior is considered by introducing an auxiliary

vector  $\mathbf{w}$  (of size  $K \times 1$ ) and assigning a gamma Markov random field prior (GMRF) for the couple  $(\boldsymbol{\sigma}, \mathbf{w})$  given by (see [14] for more details regarding this prior)

$$\begin{aligned} f(\boldsymbol{\sigma}, \mathbf{w}|\zeta) &= \frac{1}{Z(\zeta)} \left( \prod_{k=1}^K \sigma_k^{-2(2\zeta+1)} \right) \\ &\times \left( \prod_{k'=1}^K w_{k'}^{(2\zeta-1)} \right) \exp\left(\frac{-\zeta w_0}{\sigma_1^2}\right) \\ &\times \prod_{k=1}^{K-1} \exp\left[-\zeta w_k \left(\frac{1}{\sigma_k^2} + \frac{1}{\sigma_{k+1}^2}\right)\right], \end{aligned} \quad (9)$$

where  $Z(\zeta)$  is a normalizing constant and  $\zeta > 1$  is a fixed coupling parameter that controls the amount of correlation enforced by the GMRF. This prior ensures that each  $\sigma_k^2$  is connected to two neighboring elements of  $\mathbf{w}$  and vice-versa (see Fig. 2 (a)). Note that the variances  $\sigma_k^2$  and  $\sigma_{k'}^2$  for  $k \neq k'$ , are conditionally independent and that the correlation is introduced via the auxiliary variables  $\mathbf{w}$ . An interesting property of this joint prior is that the conditional prior distributions of  $\boldsymbol{\sigma}$  and  $\mathbf{w}$  reduce to conjugate inverse gamma ( $\mathcal{IG}$ ) and gamma ( $\mathcal{G}$ ) distributions, respectively, as follows [14]

$$\begin{aligned} \sigma_k^2 | w_{k-1}, w_k, \zeta &\sim \mathcal{IG}[2\zeta, \zeta(w_{k-1} + w_k)] \\ \sigma_K^2 | w_{K-1}, \zeta &\sim \mathcal{IG}(\zeta, \zeta w_{K-1}) \\ w_k | \sigma_k^2, \sigma_{k+1}^2, \zeta &\sim \mathcal{G}\left[2\zeta, \frac{1}{\zeta\left(\frac{1}{\sigma_k^2} + \frac{1}{\sigma_{k+1}^2}\right)}\right] \end{aligned} \quad (10)$$

where  $k \in \{1, \dots, K-1\}$ .

#### D. Hyperparameter priors

As previously explained, the hyperparameters  $\epsilon_k^2$  are closely related to the signal energies via the norm  $(\mathbf{s}_k^T \mathbf{H}^{-1} \mathbf{s}_k)$ . Considering this property and the continuity of the signal suggest the presence of a correlation between the parameters  $\epsilon_k^2$ . This correlation can be introduced by considering a GMRF prior for  $(\boldsymbol{\epsilon}, \mathbf{v})$  as follows [14]

$$\begin{aligned} f(\boldsymbol{\epsilon}, \mathbf{v}|\eta) &= \frac{1}{Z(\eta)} \prod_{k=1}^K \epsilon_k^{-2(2\eta+1)} \\ &\times \left( \prod_{k'=1}^K v_{k'}^{(2\eta-1)} \right) \exp\left(\frac{-\eta v_0}{\epsilon_1^2}\right) \\ &\times \prod_{k=1}^{K-1} \exp\left[-\eta v_k \left(\frac{1}{\epsilon_k^2} + \frac{1}{\epsilon_{k+1}^2}\right)\right], \end{aligned} \quad (11)$$

where  $\mathbf{v}$  are auxiliary variables and  $\eta > 1$  is the coupling parameter. A schematic description of the variable correlations is shown in Fig. 2 (b) which is similar to that presented in

Section III-C. The conjugate conditional prior distributions for  $\epsilon$  and  $\mathbf{v}$  are given by

$$\begin{aligned}\epsilon_k^2 | v_{k-1}, v_k, \eta &\sim \mathcal{IG}[2\eta, \eta(v_{k-1} + v_k)] \\ \epsilon_K^2 | v_{K-1}, \eta &\sim \mathcal{IG}(\eta, \eta v_{K-1}) \\ v_k^2 | \epsilon_k^2, \epsilon_{k+1}^2, \eta &\sim \mathcal{G}\left[2\eta, \frac{1}{\eta\left(\frac{1}{\epsilon_k^2} + \frac{1}{\epsilon_{k+1}^2}\right)}\right]\end{aligned}\quad (12)$$

where  $k \in \{1, \dots, K-1\}$ .

#### E. Posterior distributions

The proposed Bayesian model is summarized in the directed acyclic graph (DAG) displayed in Fig. 3. The parameters of interest are  $\mathbf{X} = (\mathbf{S}, \boldsymbol{\sigma}, \mathbf{w}, \epsilon, \mathbf{v})$ . The joint posterior distribution of this Bayesian model can be computed using the following hierarchical structure

$$f(\mathbf{X}|\mathbf{Y}) \propto f(\mathbf{Y}|\mathbf{S}, \boldsymbol{\sigma})f(\mathbf{S}|\epsilon)f(\epsilon, \mathbf{v})f(\boldsymbol{\sigma}, \mathbf{w}), \quad (13)$$

where we have assumed a priori independence between the parameters. For simplicity,  $f(x|\theta)$  has been denoted by  $f(x)$  when the parameter  $\theta$  is a user-fixed parameter. The MMSE and MAP estimators associated with the posterior (13) are not easy to determine. In this paper, and akin to [10], [20], we propose to evaluate the MAP estimator by using an optimization technique maximizing the posterior (13) w.r.t. the parameters of interest.

### IV. COORDINATE DESCENT ALGORITHM

This section describes the optimization algorithm maximizing the posterior (13) w.r.t. the noiseless signals and the noise variances. This provides the MAP estimator of the parameters of interest  $\mathbf{X}$ . An equivalent problem is to minimize w.r.t.  $\mathbf{X}$ , the negative log-posterior  $\mathcal{C}(\mathbf{X}) = -\log[f(\mathbf{X}|\mathbf{Y})]$  denoted as “cost function” and given by (after removing unnecessary constants)

$$\begin{aligned}\mathcal{C}(\mathbf{X}) &= \sum_{k=1}^K \left[ \left(2\zeta + \frac{M}{2} + 1\right) \log \sigma_k^2 + \frac{\beta_1}{2\sigma_k^2} - (2\zeta - 1) \log w_k \right. \\ &\quad \left. + \left(2\eta + \frac{M}{2} + 1\right) \log \epsilon_k^2 + \frac{\beta_2}{2\epsilon_k^2} - (2\eta - 1) \log v_k \right]\end{aligned}\quad (14)$$

where  $\beta_1 = \|\mathbf{y}_k - \mathbf{s}_k\|^2 + 2\zeta(w_{k-1} + w_k)$  and  $\beta_2 = \mathbf{s}_k^T \mathbf{H}^{-1} \mathbf{s}_k + 2\eta(v_{k-1} + v_k)$ . Because of the large number of parameters in  $\mathbf{X} = (\mathbf{S}, \boldsymbol{\sigma}, \mathbf{w}, \epsilon, \mathbf{v})$ , we propose a coordinate descent algorithm [15], [16] that sequentially updates the different parameters. More precisely, in



each step, the posterior distribution is maximized w.r.t. one parameter, the others being fixed. This process is repeated until the algorithm has converged to a local minimum of the cost function  $\mathcal{C}(\mathbf{S}, \boldsymbol{\sigma}, \mathbf{w}, \boldsymbol{\epsilon}, \mathbf{v})$ . Thus, the algorithm iteratively updates each parameter by maximizing its conditional distribution as described in Algo. 1. The next section describes the sub-optimization procedures maximizing the cost function  $\mathcal{C}(\mathbf{X})$  w.r.t. the noiseless signal  $\mathbf{S}$ , the noise variance  $\boldsymbol{\sigma}$  and the hyperparameters  $(\mathbf{w}, \boldsymbol{\epsilon}, \mathbf{v})$ .

---

**Algorithm 1** Smooth Signal Estimation (SSE) Algorithm

---

- 1: Input
  - 2: The noisy data  $\mathbf{Y}$ ,  $\text{zeta} > 1$ ,  $\text{eta} > 1$
  - 3: Initialization
  - 4: Initialize parameters  $\mathbf{S}^{(0)}$ ,  $\boldsymbol{\sigma}^{(0)}$ ,  $\mathbf{w}^{(0)}$ ,  $\mathbf{v}^{(0)}$ ,  $\boldsymbol{\epsilon}^{(0)}$  and  $t = 1$
  - 5: conv= 0,
  - 6: Parameter update
  - 7: **while** conv= 0 **do**
  - 8:   Update  $\mathbf{s}_k^{(t)}$ , for  $k \in \{1, \dots, K\}$  according to (31)
  - 9:   Update  $\boldsymbol{\sigma}^{(t)}$  according to (22)
  - 10:   Update  $\mathbf{w}^{(t)}$  according to (24)
  - 11:   Update  $\boldsymbol{\epsilon}^{(t)}$  according to (23)
  - 12:   Update  $\mathbf{v}^{(t)}$  according to (25)
  - 13:   Set conv= 1 if the convergence criteria are satisfied
  - 14:    $t = t + 1$
  - 15: **end while**
- 

1) *Updating the parameters:* The noiseless signal  $\mathbf{S}$  can be updated by maximizing the conditional distribution associated with each independent  $\mathbf{s}_k$ , which is a Gaussian distribution given by

$$\mathbf{s}_k | \mathbf{y}_k, \sigma_k^2, \epsilon_k^2 \sim \mathcal{N}(\overline{\mathbf{s}}_k, \boldsymbol{\Gamma}_k) \quad (15)$$

where

$$\overline{\mathbf{s}}_k = \frac{1}{\sigma_k^2} \boldsymbol{\Gamma}_k \mathbf{y}_k, \quad (16)$$

$$\boldsymbol{\Gamma}_k = \left( \frac{\mathbf{H}^{-1}}{\epsilon_k^2} + \frac{\mathbb{I}_M}{\sigma_k^2} \right)^{-1}. \quad (17)$$

Therefore, the noiseless signal  $\mathbf{S}$  can be updated using (16) which is the maximum of the Gaussian distribution. Note that this solution corresponds to a least squares solution of the quadratic problem w.r.t.  $\mathbf{s}_k$  shown in (14). Note also that the matrix inversion in (16) should be computed at each descent step leading to a high computational cost. Thus, the proposed algorithm considers a useful modification to achieve this computation with less operations, as discussed in the Appendix. The conditional distributions of  $\sigma$ , and  $\epsilon$  (resp.  $\mathbf{w}$ , and  $\mathbf{v}$ ) are inverse gamma distributions (resp. gamma distributions) as follows

$$\sigma_k^2 | \mathbf{y}_k, \mathbf{s}_k, \mathbf{w}_k \sim \mathcal{IG} \left( 2\zeta + \frac{M}{2}, \frac{\beta_1}{2} \right) \quad (18)$$

$$\epsilon_k^2 | \mathbf{y}_k, \mathbf{s}_k, \mathbf{v}_k \sim \mathcal{IG} \left( 2\eta + \frac{M}{2}, \frac{\beta_2}{2} \right) \quad (19)$$

$$w_k^2 | \sigma_k^2, \sigma_{k+1}^2, \zeta \sim \mathcal{G} \left( 2\zeta, \frac{1}{\zeta \left( \frac{1}{\sigma_k^2} + \frac{1}{\sigma_{k+1}^2} \right)} \right) \quad (20)$$

$$v_k^2 | \epsilon_k^2, \epsilon_{k+1}^2, \eta \sim \mathcal{G} \left( 2\eta, \frac{1}{\eta \left( \frac{1}{\epsilon_k^2} + \frac{1}{\epsilon_{k+1}^2} \right)} \right). \quad (21)$$

The mode of each distribution is uniquely attained and given by

$$\overline{\sigma_k^2} = \frac{\beta_1}{4\zeta + M + 2} \quad (22)$$

$$\overline{\epsilon_k^2} = \frac{\beta_2}{4\eta + M + 2} \quad (23)$$

$$\overline{w_k^2} = \frac{2\zeta - 1}{\zeta \left( \frac{1}{\sigma_k^2} + \frac{1}{\sigma_{k+1}^2} \right)} \quad (24)$$

$$\overline{v_k^2} = \frac{2\eta - 1}{\eta \left( \frac{1}{\epsilon_k^2} + \frac{1}{\epsilon_{k+1}^2} \right)}. \quad (25)$$

These modes are used to update the parameters  $\sigma, \epsilon, \mathbf{w}, \mathbf{v}$  as shown in Algo. 1.

2) *Convergence and stopping criteria:* The coordinate descent algorithm converges to a stationary point of (14) provided that the minimum of that function w.r.t.  $\mathbf{X}$  along each coordinate is unique (proposition 2.7.1 in [15]). This is easily checked for all the parameters since they have unimode conditional distributions (Gaussian, gamma and inverse-gamma distributions). The cost function is not convex, thus, the solution obtained might depend on the initial values that should be chosen carefully. In this paper, the parameters have been initialized as follows:  $\boldsymbol{\sigma}^{(0)} = \mathbf{s}_m^{(0)} = \frac{1}{M} \sum_{n=1}^M \mathbf{y}_n$ ,  $\forall m$ ,  $\epsilon_k^2 = 10$ ,  $\forall k$ , and  $w_k^{(0)} = v_k^{(0)} = 10^{-12}$ ,  $\forall k$ . Note that more elaborate initialization procedures can be investigated, but these proposed values have provided relevant results in the considered simulations (see Sections V and VI).

Algo. 1 is an iterative algorithm that requires the definition of some stopping criteria. In this paper, we have considered two criteria and the algorithm is stopped if either of them is satisfied. The first criterion compares the new value of the cost function to the previous one and stops the algorithm if the relative error between these two values is smaller than a given threshold, i.e.,

$$|\mathcal{C}(\mathbf{X}^{t+1}) - \mathcal{C}(\mathbf{X}^t)| \leq \xi \mathcal{C}(\mathbf{X}^t), \quad (26)$$

where  $|\cdot|$  denotes the absolute value and  $\xi$  is the threshold that has been fixed to  $\xi = 0.001$ . The second criterion is based on a maximum number of iterations  $T_{\max} = 100$ . The next sections study the behavior of the proposed algorithm when considering synthetic and real signals.

## V. VALIDATION ON SYNTHETIC DATA

This section evaluates the performance of the proposed algorithm with synthetic data. It is divided into two parts whose objectives are: 1) introducing the criteria used for the evaluation of the algorithm quality, 2) analyzing and comparing the behavior of the proposed algorithm with other state-of-the-art algorithms.

### A. Evaluation criteria

For synthetic signals, the quality of the proposed algorithm can be evaluated by comparing the noiseless signals  $\mathbf{s}_m$  to the denoised signals  $\hat{\mathbf{s}}_m$  using the reconstruction signal to noise ratio (RSNR) given by [21]

$$\text{RSNR} = 10 \log_{10} \left( \frac{\sum_{m=1}^M \|\mathbf{s}_m\|^2}{\sum_{m=1}^M \|\mathbf{s}_m - \hat{\mathbf{s}}_m\|^2} \right). \quad (27)$$

Note that a high RSNR corresponds to a good denoising result. Moreover, the true altimetric parameters are known for synthetic signals. Thus, the true values can be compared to the estimated ones before and after filtering to highlight the benefit of the proposed denoising algorithm. Note that the altimetric parameters have been estimated using the well known least-squares (LS) based strategy that is commonly used by the altimetric community [6], [10]. The quality of the estimated parameters is evaluated using the root mean square error

(RMSE) and the standard deviations (STDs) of the estimator  $\hat{\theta}_i$  as follows

$$\text{RMSE}(\hat{\theta}_i) = \sqrt{\frac{1}{N} \sum_{n=1}^N [\hat{\theta}_i(n) - \theta_i(n)]^2}, \quad (28)$$

$$\text{STD}(\hat{\theta}_i) = \sqrt{\frac{1}{N} \sum_{n=1}^N \left[ \hat{\theta}_i(n) - \left( \frac{1}{N'} \sum_{n'=1}^{N'} \hat{\theta}_i(n') \right) \right]^2} \quad (29)$$

for  $i \in \{1, \dots, 3\}$ , where  $\theta_i(n)$  (resp.  $\hat{\theta}_i(n)$ ) is the true (resp. estimated) parameter for the  $n$ th signal and  $N$  is the number of simulated signals ( $N' = N$  for synthetic signals).

When considering real signals, the performance of the proposed algorithm is qualitatively evaluated by a visual comparison between the noisy signals/parameters and the denoised ones [6], [9], [10]. Quantitatively, a modified parameter STD is computed using (29) in which the averaged parameter value is approached by the mean of the estimated parameters along each  $N' = 20$  successive signals. This modified STD is called “STD at 20 Hz” [13], [22]–[24].

### B. Simulation results on synthetic data

Two experiments are conducted to evaluate the performance of the proposed SSE (for smooth signal estimation) algorithm. The first experiment studies the behavior of SSE when varying the number of the denoised signals  $M$ . Indeed, the SSE algorithm considers successive sets of length  $M$  to denoise the observed altimetric signals. Therefore,  $N = 5000$  signals are generated according to the altimetric model (3) while using a realistic variation of the altimetric parameters  $\Theta_m = [\text{SWH}(m), \tau(m), P_u(m)]$ . This realistic sequence of parameters is obtained by applying the CD-BM algorithm [10], on 5000 real Jason-2 signals (since it provides physically realistic smooth parameters) where we obtain  $\text{SWH} \in [3.4, 5.4]\text{m}$ ,  $\tau \in [14.3, 15]\text{ m}$  and  $P_u \in [150, 190]\text{ unit}$  (see Fig. 4 black lines). The generated synthetic signals are then corrupted by speckle noise resulting from the averaging of  $L = 90$  signals and leading to  $\text{RSNR} = 19.55\text{ dB}$ . The obtained  $N = 5000$  signals are processed by the proposed algorithm while considering different set lengths as shown in Table I. For example, for a length set  $M = 250$ , the algorithm is run 20 times to process the  $N = 5000$  signals. Overall, these results show an  $\approx 11\text{ dB}$  improvement in the processed data with an increasing  $\text{RSNR}$  w.r.t.  $M$ . However, a high number of  $M$  requires higher computational cost (mainly due to the matrix inversion in (16)), while too small  $M$  leads to more iterations. The value  $M = 500$  represents a good compromise and we consider this value for the rest of the paper [10].

The second experiment studies the effect of the algorithm on the physical altimetric parameters ( $\text{SWH}$ ,  $\tau$ ,  $P_u$ ). Indeed, it is of interest to devote more effort to improve the quality of the estimated altimetric parameters and to reduce the parameter standard-deviations [8]–[10], [13], [24]. These parameters are estimated using the well known least-squares (LS) based strategy [6], [10] applied to noisy and filtered signals. The proposed strategy (denoted as SSE-LS) is compared to the classical LS algorithm (without filtering) [6], [10], and to SVD-LS which is obtained by applying the singular value decomposition filtering strategy [11], [12] (with a threshold equal to 84%) followed by the LS algorithm. Following [3], [24], the study is performed when varying  $\text{SWH} \in [0.5, 8]$  m with fixed  $\tau = 31$  gates and  $P_u = 130$ . For each SWH, 500 synthetic signals are generated using the Brown model with different noise realizations (500 Monte carlo runs) and processed using the three considered algorithms. Fig. 5 presents the obtained parameter RMSEs w.r.t. SWH when considering the LS, SVD-LS and SSE-LS strategies. Overall, the proposed strategy presents the best performance with the lowest RMSEs. Indeed, at a typical SWH of 2 m, the proposed SSE-LS reduces  $\text{RMSE}(\text{SWH})$  to 10 cm (against 40 cm and 20 cm for LS and SVD-LS),  $\text{RMSE}(\tau)$  to 1cm (against 6 cm and 2.3 cm for LS and SVD-LS) and  $\text{RMSE}(P_u)$  to 0.6 (against 2 and 1.8 for LS and SVD-LS). This parameter improvement is also highlighted in Fig. 4 which shows the estimated parameters when considering the first experiment settings (for clarity purpose, we only show 1200 signal parameters). It is clear from this figure that SSE-LS (blue lines) provides smoother results that better approximate the actual parameters (black lines) than LS (red lines) and SVD-LS (green lines). Table II reports the obtained RSNR when considering SVD-LS and SSE-LS for different SWH. This table shows an average improvement by 6 dB when considering SVD-LS and by 12 dB when considering the proposed SSE-LS algorithm. It also shows a slightly decreasing performance for SVD-LS when increasing SWH while SSE-LS provides almost similar RSNR for all SWH. These results highlight the interest of the proposed strategy in denoising the altimetric signals and improving the estimated altimetric parameters.

## VI. RESULTS ON JASON-2 REAL DATA

This section is devoted to the validation of the proposed SSE denoising algorithm when applied to the oceanic Jason-2 dataset. The data considered last for a period of 36 minutes and consist of 43000 real signals that were extracted from pass 30 of cycle 35. Fig. 6 presents a sequence of 800 Jason-2 signals before and after filtering. Note first that this sequence shows

a reduced variation in the altimetric signals which justifies the use of the proposed strategy. Moreover, it clearly shows a reduction in the noise affecting the signals after the application of the SSE algorithm especially in the tail of the signal (the decreasing part), which was most affected by the speckle noise. Fig. 7 shows the parameters estimated w.r.t. time when considering the LS (in red), SVD-LS (in green) and SSE-LS (in blue) algorithms. As observed for synthetic data in Section V-B, the proposed SSE-LS provides a smooth parameter evolution which is physically more consistent, while SVD-LS and LS present high estimation noise (a lot of vibrations especially for  $P_u$ ). This result is quantitatively confirmed in Table III which shows smaller STDs for SSE-LS than for LS and SVD-LS. This STD reduction is of great importance for many practical applications related to oceanography such as bathymetry. Comparing SSE-LS to LS, Table III highlights an STD improvement factor by 6 for SWH, 4 for  $\tau$  and 5 for  $P_u$ . This table also shows a good agreement between the means of the estimated parameters for the LS, SVD-LS and SSE-LS algorithms (except  $P_u$  that is slightly reduced by SSE-LS as shown in Fig. 7). Finally, Table III also compares the computational costs of the three considered algorithms when processing the 43000 signals (the result is reported for each signal). Because of the filtering step, both SVD-LS and SSE-LS require more computational times than LS. Note that the proposed SSE algorithm requires more computational time than the SVD approach. However, this cost (about 12% of additional computational times w.r.t. the LS algorithm) must be balanced by the performance improvement in terms of RSNR and parameter STDs. These results confirm the good performance of the proposed strategy for denoising smooth signals such as oceanic altimetric signals.

## VII. CONCLUSIONS

This paper has presented a new Bayesian strategy for the estimation of smooth signals corrupted by Gaussian noise. The successive continuous signals can have a numerical expression or be given by a linear/nonlinear function with respect to some parameters. A Bayesian model was proposed to take into account the Gaussian properties of the noise and the smooth properties of the signal evolutions. Moreover, the signal energies were assigned a GMRF prior that introduces correlation between their values to account for their continuity. Similarly, the noise variances were also assigned a GMRF to better approximate the speckle noise that can affect the signals. The resulting posterior distribution was maximized using a fast coordinate descent algorithm that showed good results on both synthetic and real altimetric signals. The proposed algorithm was also evaluated by combining it with a commonly used parameter

estimation strategy for the altimetric parameters. The estimated parameters showed a clear improvement highlighting the benefit of the proposed algorithm. It is worth-noting that the proposed strategy is fast and generic and thus could be applied when considering other altimetric technologies such as delay/Doppler altimetry [5], [13], [24]. This point will be considered in future work. Generalizing the proposed approach for hyperspectral images is also an interesting issue that is currently under investigation.

## APPENDIX

### MATHEMATICAL DERIVATIONS

#### A. Updating the noiseless signal $\mathbf{s}_k$

The  $(M \times M)$  matrix inversion in (17) should be computed at each update of the noiseless signals which requires a high computational cost. To avoid this cost, we divide this matrix inversion into two parts. One representing the heavy computations and is achieved outside the “while” loop in Algo. 1. The other one includes simple vector multiplications and is kept inside the loop. To achieve this, an SVD decomposition is first applied to  $\mathbf{H}^{-1}$  as follows

$$\mathbf{H}^{-1} = \mathbf{V} \mathbf{D}(r_i) \mathbf{V}^T \quad (30)$$

where  $\mathbf{D}(x_i)$  denotes a diagonal matrix with its  $i$ th diagonal element equal to  $x_i$ ,  $r_i$  is the  $i$ th singular value of  $\mathbf{H}^{-1}$  and  $\mathbf{V}$  is a unitary orthogonal matrix, i.e.,  $\mathbf{V}\mathbf{V}^T = \mathbb{I}_M$ . Straightforward computations lead to the following expression for the noiseless signal update

$$\overline{\mathbf{s}}_k = \mathbf{V} \mathbf{D} \left( \frac{\epsilon_k^2}{r_i \sigma_k^2 + \epsilon_k^2} \right) \underline{\mathbf{V}^T \mathbf{y}_k}. \quad (31)$$

Note that the operation underlined in (31) and the SVD decomposition (30) are only computed once outside the loop while the remaining vector operations in (31) are achieved inside the loop.



## REFERENCES

- [1] B. W. Hapke, "Bidirectional reflectance spectroscopy. I. Theory," *J. Geophys. Res.*, vol. 86, pp. 3039–3054, 1981.
- [2] G. Brown, "The average impulse response of a rough surface and its applications," *IEEE Trans. Antennas and Propagation*, vol. 25, no. 1, pp. 67–74, Jan. 1977.
- [3] A. Halimi, C. Mailhes, J.-Y. Tourneret, P. Thibaut, and F. Boy, "Parameter estimation for peaky altimetric waveforms," *IEEE Trans. Geosci. Remote Sens.*, vol. 51, no. 3, pp. 1568–1577, March 2013.
- [4] P. Vincent, N. Steunou, E. Caubet, L. Phalippou, L. Rey, E. Thouvenot, and J. Verron, "AltiKa: a Ka-band altimetry payload and system for operational altimetry during the GMES period," *Sensors*, vol. 6, no. 3, pp. 208–234, Mar. 2006.
- [5] R. K. Raney, "The delay/Doppler radar altimeter," *IEEE Trans. Geosci. Remote Sens.*, vol. 36, no. 5, pp. 1578–1588, Sept. 1998.
- [6] L. Amarouche, P. Thibaut, O. Z. Zanife, J.-P. Dumont, P. Vincent, and N. Steunou, "Improving the Jason-1 ground retracking to better account for attitude effects," *Marine Geodesy*, vol. 27, no. 1-2, pp. 171–197, Aug. 2004.
- [7] A. Halimi, "From conventional to delay/doppler altimetry," Ph.D. dissertation, Institut National Polytechnique de Toulouse, Toulouse, France, 2013. [Online]. Available: <http://ethesis.inp-toulouse.fr/archive/00002423/01/halimi.pdf>
- [8] S. Maus, C. M. Green, and J. D. Fairhead, "Improved ocean-geoid resolution from retracked ERS-1 satellite altimeter waveforms," *Geophysical Journal International*, vol. 134, no. 1, pp. 243–253, Feb. 1998.
- [9] D. T. Sandwell and W. H. F. Smith, "Retracking ERS-1 altimeter waveforms for optimal gravity field recovery," *Geophys. J. Int.*, vol. 163, no. 1, pp. 79–89, Oct. 2005.
- [10] A. Halimi, C. Mailhes, J.-Y. Tourneret, and H. Snoussi, "Bayesian estimation of smooth altimetric parameters: Application to conventional and delay/Doppler altimetry," *IEEE Trans. Geosci. Remote Sens.*, 2016, to appear.
- [11] A. Ollivier, "Nouvelle approche pour l'extraction de paramtres gophysiques partir des mesures en altimtrie radar," Ph.D. dissertation, Institut National Polytechnique de Grenoble, Grenoble, France, 2006.
- [12] P. Thibaut, J. Poisson, A. Ollivier, E. Bronner, and N. Picot, "Singular value decomposition applied on altimeter waveforms," in *Report of the Ocean Surf. Topogr. Sci. Team Meet. (OSTST)*, Seattle, USA, June 2009. [Online]. Available: [http://www.aviso.altimetry.fr/fileadmin/documents/OSTST/2009/oral/Thibaut\\_SVD2.pdf](http://www.aviso.altimetry.fr/fileadmin/documents/OSTST/2009/oral/Thibaut_SVD2.pdf)
- [13] A. Halimi, C. Mailhes, J.-Y. Tourneret, P. Thibaut, and F. Boy, "A semi-analytical model for delay/Doppler altimetry and its estimation algorithm," *IEEE Trans. Geosci. Remote Sens.*, vol. 52, no. 7, pp. 4248–4258, July 2014.
- [14] O. Dikmen and A. Cemgil, "Gamma markov random fields for audio source modeling," *IEEE Trans. Audio, Speech, Language Process.*, vol. 18, no. 3, pp. 589–601, March 2010.
- [15] D. P. Bertsekas, *Nonlinear programming*. Belmont, Massachusetts: Athena Scientific, 1995.
- [16] J. Sigurdsson, M. Ulfarsson, and J. Sveinsson, "Hyperspectral unmixing with  $l_q$  regularization," *IEEE Trans. Geosci. Remote Sens.*, vol. 52, no. 11, pp. 6793–6806, Nov. 2014.
- [17] C. Martin-Puig and G. Ruffini, "SAR altimeter retracker performance bound over water surfaces," in *Proc. IEEE Int. Conf. Geosci. Remote Sens. (IGARSS)*, Cape Town, South Africa, July 12-17, 2009, pp. 449–452.
- [18] O. Germain and G. Ruffini, "A revisit to the GNSS-R code range precision," in *Proc. GNSS-R*, Noordwijk, The Netherlands, June 14-15, 2006.
- [19] A. Halimi, C. Mailhes, and J.-Y. Tourneret, "Cramér-Rao bounds and estimation algorithms for delay/Doppler and conventional altimetry," in *Proc. EUSIPCO*, Marrakech-Marocco, Sept. 9-13 2013.
- [20] A. Halimi, P. Honeine, and J. M. Bioucas-Dias, "Hyperspectral unmixing in presence of endmember variability, nonlinearity or mismodelling effects," in *ArXiv e-prints*, Nov. 2015.

- [21] J. Bioucas-Dias and M. Figueiredo, "Alternating direction algorithms for constrained sparse regression: Application to hyperspectral unmixing," in *Proc. IEEE GRSS Workshop on Hyperspectral Image and Signal Processing: Evolution in Remote Sensing (WHISPERS)*, June 2010, pp. 1–4.
- [22] K. Giles, D. Wingham, N. Galin, R. Cullen, and W. Smith, "Precise estimates of ocean surface parameters from cryosat," in *Report of the Ocean Surf. Topogr. Sci. Team Meet. (OSTST)*, Venice-Lido, Italy, Sept. 22-29, 2012. [Online]. Available: [http://www.aviso.oceanobs.com/fileadmin/documents/OSTST/2012/oral/02\\_friday\\_28/05\\_instr\\_processing\\_Ilb/02\\_IP2B\\_Giles.pdf](http://www.aviso.oceanobs.com/fileadmin/documents/OSTST/2012/oral/02_friday_28/05_instr_processing_Ilb/02_IP2B_Giles.pdf)
- [23] C. Gommenginger, C. Martin-Puig, S. Dinardo, D. Cotton, M. Srokosz, and J. Benveniste, "Improved altimetric accuracy of SAR altimeters over the ocean: observational evidence from Cryosat-2 SAR and Jason-2," in *Report of the Ocean Surf. Topogr. Sci. Team Meet. (OSTST)*, San Diego, California, Oct. 19-21, 2011. [Online]. Available: [http://www.aviso.oceanobs.com/fileadmin/documents/OSTST/2011/oral/01\\_Wednesday/Splinter%201%20IP/01%20Gommenginger%20SAMOSA\\_OSTST\\_Oct2011.pdf](http://www.aviso.oceanobs.com/fileadmin/documents/OSTST/2011/oral/01_Wednesday/Splinter%201%20IP/01%20Gommenginger%20SAMOSA_OSTST_Oct2011.pdf)
- [24] A. Halimi, C. Mailhes, J.-Y. Tournet, T. Moreau, and F. Boy, "Including antenna mispointing in a semi-analytical model for delay/Doppler altimetry," *IEEE Trans. Geosci. Remote Sens.*, vol. 53, no. 2, pp. 598–608, Feb. 2015.

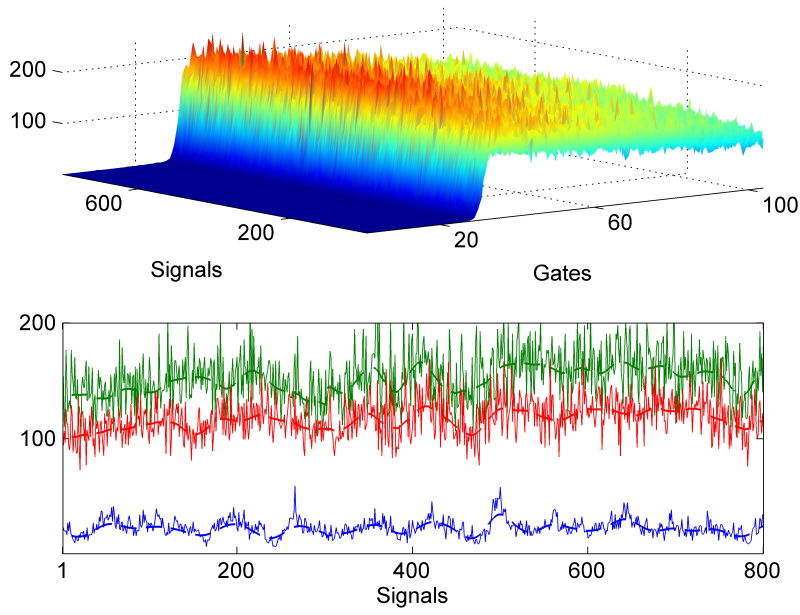


Fig. 1. (Top) Example of 800 noisy Jason-2 signals. (Bottom) Signal evolutions in gates (30, 50, 90) (continuous lines) and their smooth approximation with the proposed SSE algorithm (dashed lines).

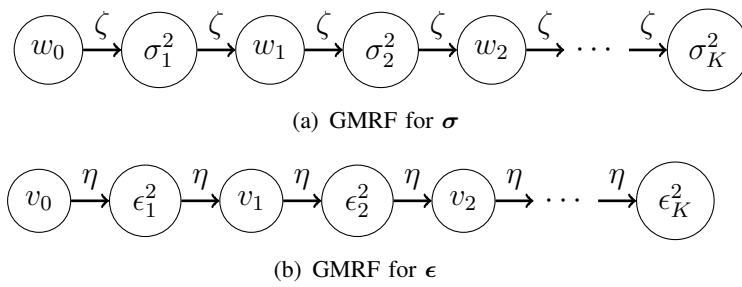


Fig. 2. Proposed 1st order GMRF neighborhood structures for (a) the noise variances  $\sigma$  and (b) the signal energies  $\epsilon$ .

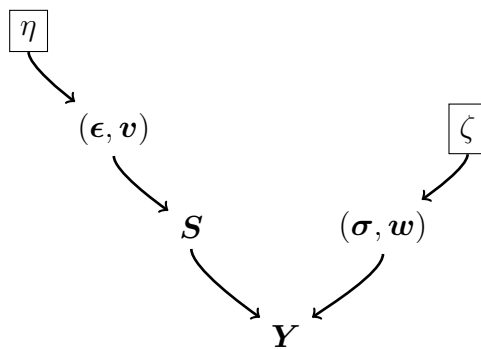
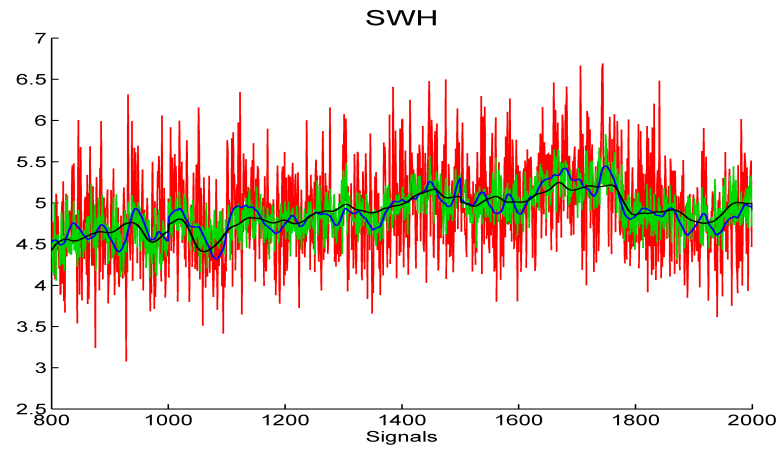


Fig. 3. DAG for the parameter and hyperparameter priors (the user-fixed parameters appear in boxes).



(a) SWH

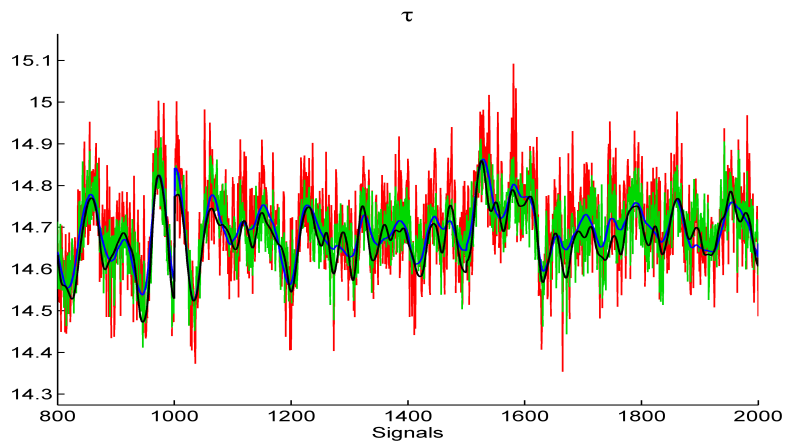
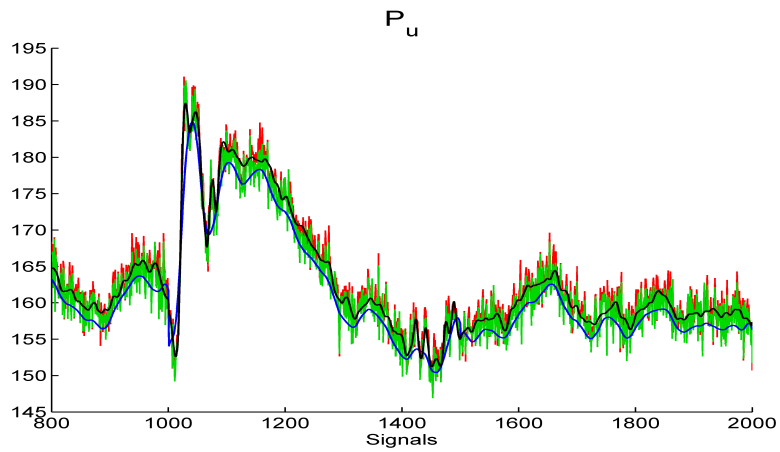
(b)  $\tau$ (c)  $P_u$ 

Fig. 4. Example of 1200 ground-truth synthetic parameters (black lines) and their estimations using the LS algorithm (red line), the SVD-LS algorithm with  $M = 500$  (green line) and the proposed SSE-LS algorithm with  $M = 500$  (blue line). (a) SWH, (b)  $\tau$  and (c)  $P_u$ .

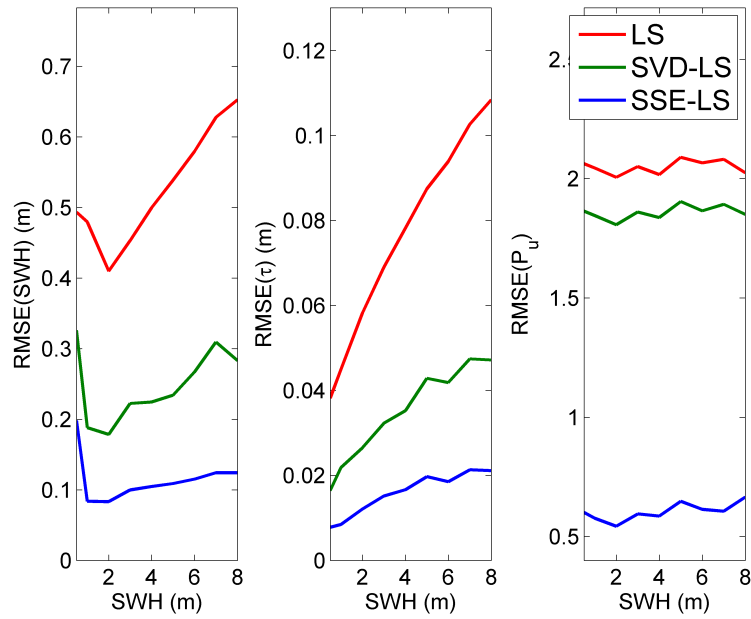


Fig. 5. RMSEs of the altimetric parameters w.r.t. SWH for LS, SVD-LS and SSE-LS algorithms.

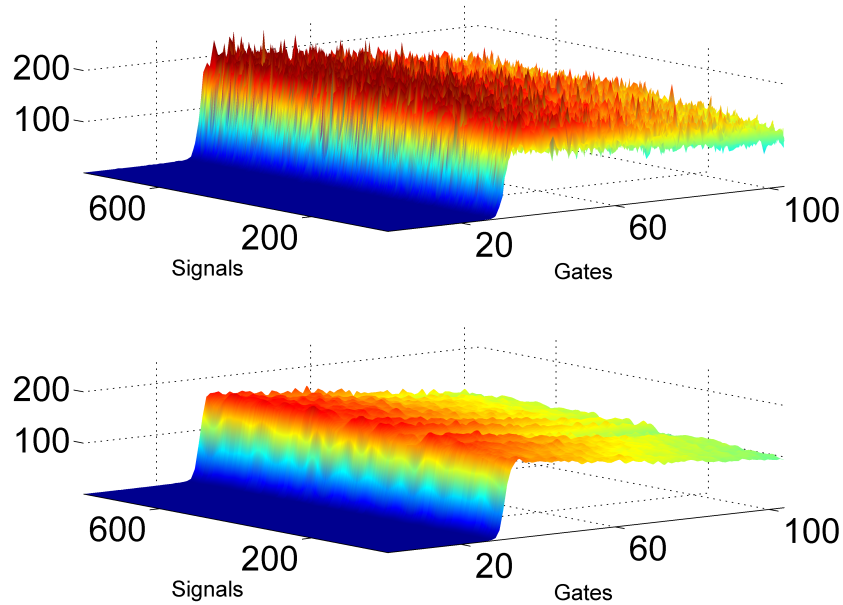
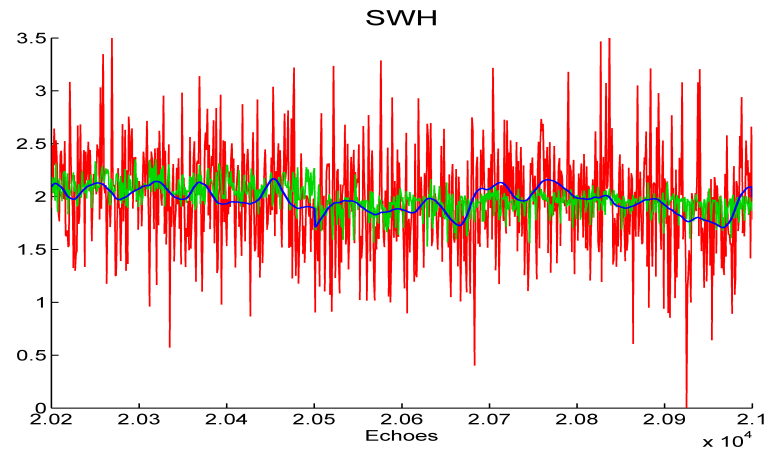


Fig. 6. Example of Jason-2 echoes. (top) without filtering and (bottom) with SSE filtering.



(a) SWH

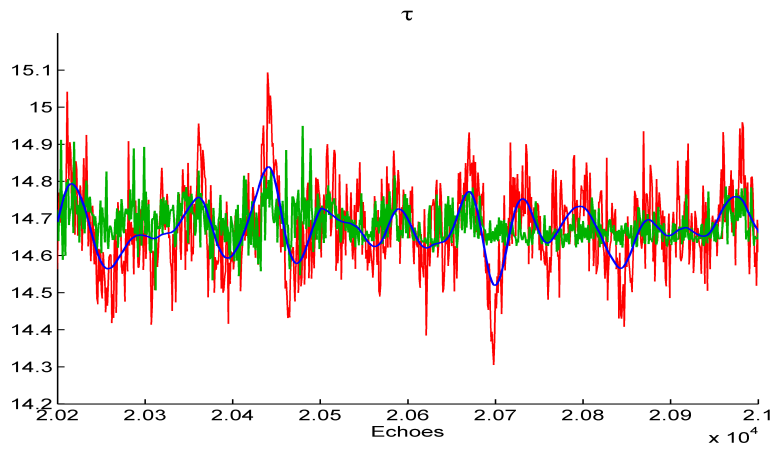
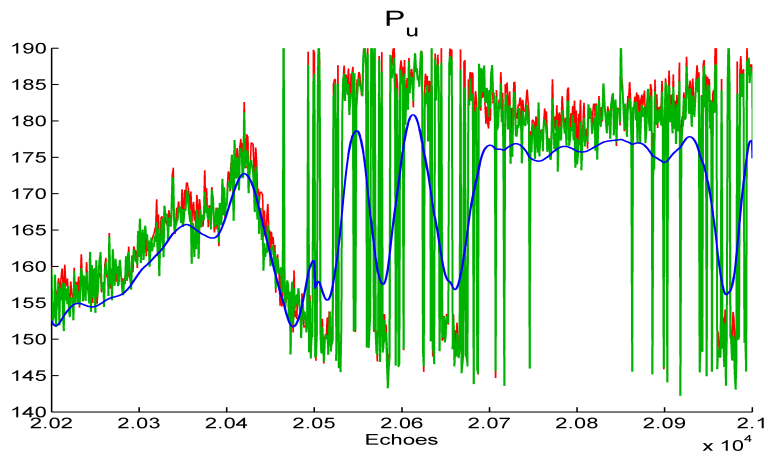
(b)  $\tau$ (c)  $P_u$ 

Fig. 7. Estimated parameters using the LS algorithm (red line), the SVD-LS algorithm (green line) and the proposed SSE-LS algorithm (blue line) for Jason-2 signals. (a) SWH, (b)  $\tau$  and (c)  $P_u$ .

TABLE I  
PERFORMANCE OF THE PROPOSED SSE ALGORITHM W.R.T. THE FILTER LENGTH (5000 SIGNALS). THE CORRUPTED DATA PRESENTS AN  $\text{RSNR} = 19.55\text{dB}$ .

	Filter length						
	50	100	250	500	1000	2500	5000
RSNR (dB)	31.1	31.4	31.5	31.6	31.7	31.7	31.7
Time per signal (ms)	0.35	0.24	0.25	0.38	1.03	5.00	17.47

TABLE II  
RSNR (IN dB) WITH RESPECT TO SWH. THE CORRUPTED DATA PRESENTS AN  $\text{RSNR} = 19.55\text{dB}$ .

		SWH (m)								
		0.5	1	2	3	4	5	6	7	8
RSNR (dB)	SVD-LS	26.35	26.43	26.30	26.02	26.03	26.07	26.08	25.92	25.86
	SSE-LS	32.24	32.21	32.22	32.13	32.15	32.10	32.22	32.13	32.07

TABLE III  
PERFORMANCE ON REAL JASON-2 DATA (45000 SIGNALS).

		SWH (cm)	$\tau$ (cm)	$P_u$
Mean	LS	242	14.68	167.73
	SVD-LS	241	14.67	166.62
	SSE-LS	248	14.68	164.83
STD	LS	59.9	12.01	6.18
	SVD-LS	18.14	6.02	6.09
	SSE-LS	<b>9.03</b>	<b>2.94</b>	<b>1.21</b>
Average time per signal (ms)	LS	<b>8.56</b>		
	SVD-LS	9.05		
	SSE-LS	9.63		